Final state interactions and relativistic effects in y scaling

C. R. Chinn
Department of Physics and Astronomy,
Vanderbilt University, Nashville, Tennessee 37235
(Received 29 April 1994)

The role of final state interactions in y scaling in quasielastic electronuclear reactions is investigated in a physically realistic model, which incorporates the final state interactions via the optical model Green's function. Relativistic and nonrelativistic complex optical potentials are utilized in finite nucleus, fully-off-shell, momentum space calculations to represent the final state interactions in an approach which has been shown to provide realistic descriptions of the separate response functions in the inclusive reaction. Analyses of the effects of Dirac dynamical degrees of freedom and final state interactions upon the separate longitudinal and transverse scaling functions are presented along with a discussion of the high momentum transfer dependence.

PACS number(s): 25.30.−c, 25.30.Fj, 24.10.Ht, 24.10.Jv

I. INTRODUCTION

The study of y scaling in electronuclear physics has become a popular topic among both experimentalists and theorists [1]. y scaling analyses provide a compact and straightforward platform for analyzing experimental results, where the possibility of extracting the nuclear momentum distribution has been investigated [2]. In the cases with unexpected y scaling behavior, excellent opportunities for studying and searching for physical contributions arise due to overlooked or unusual degrees of freedom.

Recent comments have been made about the contributions of final state interactions [FSI] in y scaling [3–6]. From studies of the separated inclusive response functions in quasielastic (e, e') reactions, it has been shown that FSI provide large effects in a range of momentum transfers [7, 8]. Using model eikonal, local, and nuclear matter calculations, FSI have also been shown to play a possibly significant role in y scaling [5, 6]. In this paper a model, which introduces a complex, nonlocal, off-shell optical potential to study the FSI in a relativistic finite nucleus calculation, is used. It is hoped that the use of such a model, which gives a realistic and accurate description of the separated quasielastic response functions, will provide a clearer understanding of the role and behavior of FSI in the y scaling regime.

Suggestions that the y scaling properties of nuclei are such that it may be possible to retrieve the nuclear momentum distributions and effects due to correlations from the experimental structure functions [1]. This concept, of course, relies on one's ability to reduce any ambiguities which may arise in the data as a result of effects external to the y scaling hypothesis. Hence, the motivation of this paper is to use a physically realistic model to try and unravel theoretically the role of FSI in y scaling.

When the experimental results are interpreted in terms of the differential cross section, it is found that y scaling is generally obeyed. Recently, analyses have been performed in terms of the separated response functions, where it was found that the previous well-behaved y scaling interpretation becomes less clear. For the longitudinal response R_L, one can look at both regions, $y < 0$ and $y > 0$. Since R_L is coupled more directly to the charge and hence the density, one would naively expect R_L to scale better than the transverse response R_T. This was found to be untrue. R_T scales reasonably well, while R_L does not.

A theoretical discussion of the plane wave approximation [PWA] and FSI calculations for the quasielastic (e, e') reaction and the separated y scaling functions is given in Sec. II. The results for the calculation of the scaling functions are presented in Sec. III. Section IV contains an analysis of the FSI contributions as a function of $|\mathbf{q}|^{-1}$ followed by a summary and conclusion.

II. THEORETICAL DISCUSSION

The y scaling variable itself is not unambiguous. There have been a number of investigations and surveys of the various constructions of y [9]. In this paper we have chosen to use the variable introduced in Ref. [10] and discussed in detail in Ref. [3]. This variable derives from the conservation of relativistic energy and includes some of the effects due to the average binding energy of the target nucleons.

$$\omega = \sqrt{m^2 + (|\mathbf{q}| + y)^2} + \sqrt{M_{A-1}^2 + y^2} - M_A \geq E_s, \tag{1}$$

$$M_{A-1} = M_A - m + E_s. \tag{2}$$

Here E_s is taken to be the average binding energy and M_A is the mass of the target nucleus. The four momentum transferred by the scattering electron is given by $q = (\omega, \mathbf{q})$. Equivalently, the y variable can be expressed as [10]

$$y = \frac{-|\mathbf{q}|\,\lambda + (\omega + M_A)\sqrt{\lambda^2 - W^2 M_{A-1}^2}}{W^2}, \quad (3)$$
$$W^2 = (\omega + M_A)^2 - |\mathbf{q}|^2,$$
$$\lambda = \frac{1}{2}\left[-m^2 + M_{A-1}^2 + W^2\right].$$

We have chosen not to discuss the different functional choices for y, and instead to investigate the behavior of a particular model description of the nuclear reaction mechanism in the y scaling regime.

In recent experimental measurements of ^{3}He and ^{4}He, a y scaling analysis was performed in terms of the separated response functions [11]. Scattering from ^{3}He and ^{4}He traditionally is addressed with a few-body physical model. Since larger nuclei involve stronger nuclear fields and larger binding energies, experimental measurements using larger nuclear targets would encounter stronger FSI and off-shell effects. In the initial studies of the separated response functions of the quasielastic (e, e') reactions, it was found that although simple Fermi gas calculations were able to reproduce reasonably well the doubly differential cross sections, it was not possible to predict simultaneously both response functions. This led to much effort to try to resolve this discrepancy, in which more sophisticated models and calculations were performed. A similar story may unfold in studies of the separated scaling functions, where one expects that for large values of the momentum transfer $|\mathbf{q}|$, these functions should become independent of $|\mathbf{q}|$.

In this paper the separated scaling functions are defined as [12]

$$F_L(\mathbf{q}, y) \equiv \eta \frac{R_L(\mathbf{q}, \omega)}{ZW_L(p) + NW_L(n)},$$
$$F_T(\mathbf{q}, y) \equiv \eta \frac{R_T(\mathbf{q}, \omega)}{ZW_T(p) + NW_T(n)}, \quad (4)$$

where

$$\eta = \frac{1}{|\mathbf{k}|}\left|\frac{\partial\omega}{\partial\cos\theta_k}\right| = \frac{|\mathbf{q}|}{\sqrt{m^2 + (|\mathbf{q}| + y)^2}}.$$

The numbers Z and N correspond to the proton and neutron numbers, respectively, while $\cos\theta_k$ is the angle between $\mathbf{k}$ and $\mathbf{q}$. The structure functions W_L and W_T are calculated relativistically in the Born approximation as the elastic scattering of electrons from a free nucleon:

$$W^{\mu\nu} = \mathrm{Tr}\left\{\frac{\not{p}' + m}{2E_{p'}}\hat{J}^{\mu\dagger}(q)\frac{\not{p} + m}{2E_p}\hat{J}^{\nu}(q)\right\}. \quad (5)$$

The proton and neutron longitudinal and transverse contributions are defined as $W_L \equiv W^{00}$ and $W_T \equiv W^{11} + W^{22}$. Choosing particular forms for the current operators, one finds the following expressions:

$$W_L = \frac{1}{4E_{p'}E_p}\left\{-2\mathbf{q}^2\left(F_1(q^2) + F_2(q^2)\right)^2 + 2\left(E_p + E_{p'}\right)^2\left[F_1(q^2)^2 - \bar{q}^2\left(\frac{F_2(q^2)}{2m}\right)^2\right]\right\}, \quad (6)$$

$$W_T^{cc2} = \frac{1}{E_{p'}E_p}\left\{F_1(q^2)^2\left[2E_pE_{p'} - 2m^2 + \frac{\mathbf{q}^2}{2} - \frac{\bar{\omega}^2\left(E_p + E_{p'}\right)^2}{2\mathbf{q}^2}\right]\right.$$
$$-2F_1(q^2)F_2(q^2)\bar{q}\cdot q + \left(\frac{F_2(q^2)}{2m}\right)^2\left[(\omega^2 - \mathbf{q}^2)\left(-E_p^2 - E_{p'}^2\right.\right.$$
$$\left.\left.-2m^2 + \frac{\mathbf{q}^2}{2} + \frac{\bar{\omega}^2\left(E_p + E_{p'}\right)^2}{2\mathbf{q}^2}\right) + (\omega - \bar{\omega})^2\left(\left(E_p + E_{p'}\right)^2 - \mathbf{q}^2\right)\right]\right\}, \quad (7)$$

$$W_T^{cc1} = \frac{1}{E_{p'}E_p}\left\{-\left(F_1(q^2) + F_2(q^2)\right)^2\bar{q}^2 + \left(F_1(q^2)^2 - \bar{q}^2\left(\frac{F_2(q^2)}{2m}\right)^2\right)\left[E_p^2 + E_{p'}^2 - \frac{\mathbf{q}^2}{2} - 2m^2 - \frac{\bar{\omega}^2\left(E_p + E_{p'}\right)^2}{2\mathbf{q}^2}\right]\right\}, \quad (8)$$

where the variables $\bar{\omega}$ and $\bar{q}$ use the nucleon on-shell energies in the following fashion: $\bar{\omega} = E_{p'} - E_p$, $\bar{q}^2 = \bar{\omega}^2 - \mathbf{q}^2$. The superscripts will be described in more detail later, where $cc1$ refers to the de Forest [13] choice of the current operator and $cc2$ refers to the standard Dirac current operator.

Final state interactions are calculated using the Green's function doorway approach to (e, e') quasielastic scattering [7]. For a more complete discussion, please see Ref. [8]. The longitudinal and transverse response functions within the one-photon-exchange approximation are given by

$$R_L(\mathbf{q}, \omega) = W^{00}(\mathbf{q}, \omega),$$
$$R_T(\mathbf{q}, \omega) = W^{11}(\mathbf{q}, \omega) + W^{22}(\mathbf{q}, \omega), \quad (9)$$

where

$$W^{\mu\nu} = \overline{\sum_i}\sum_f \langle i|\hat{J}^{\mu}(q)^{\dagger}|f\rangle\delta(E_i + \omega - E_f)\langle f|\hat{J}^{\nu}(q)|i\rangle. \quad (10)$$

Here $|i\rangle$ represents the initial nuclear many-body state, while the sum over $|f\rangle$ corresponds to all final states of the full hadronic many-body assembly. $\hat{J}^{\mu}(q)$ is the elec-

tromagnetic nuclear current operator and the $\overline{\sum_i}$ denotes an average over the initial states.

One would like to perform an explicit sum over the complete set of complex inelastic reaction channels in the final state, but in practice such a many-body calculation is prohibitively difficult. By focusing on the scattering spectrum, a one-body approximation to the current operator can be used to simplify the problem which will still include much of the physical reactive content necessary to provide a reasonable and consistent description.

Suppressing the discrete state contribution, Eq. (10) can be rewritten in terms of the forward virtual Compton amplitude:

$$W^{\mu\nu}(\mathbf{q},\omega) = -\frac{1}{\pi}\mathrm{Im}\,T^{\mu\nu}(\mathbf{q},\omega), \tag{11}$$

where

$$T^{\mu\nu}(\mathbf{q},\omega) = \overline{\sum_i}\langle i|\hat{J}^{\mu}(q)^{\dagger}\hat{G}(\omega+E_i)\hat{J}^{\nu}(q)|i\rangle. \tag{12}$$

Here $\hat{G}$ is the full many-body propagator for the A-nucleon system. If $\hat{J}^{\mu}$ is assumed to be a one-body operator, it can be shown [8] that $\hat{G}$ reduces to the optical model Green's function, which maintains a proper and consistent unitary description of the reactive content of this inclusive reaction. If one assumes that each knockout channel is represented by the same optical model potential, then the following substitution can be made:

$$\hat{G} \approx \hat{G}_{\mathrm{opt}} = \hat{G}_0 + \hat{G}_0\,\hat{U}_{\mathrm{opt}}\,\hat{G}_{\mathrm{opt}}. \tag{13}$$

$\hat{G}_{\mathrm{opt}}$ then corresponds to using an optical model potential to represent the final state interactions between the ejected nucleon and the residual nucleus. $\hat{G}_0$ is the free propagator for a nucleon within the nuclear medium.

To reduce the calculation to the PWA, $\hat{U}_{\mathrm{opt}}$ is set to zero or equivalently,

$$\hat{G} \approx \hat{G}_0, \tag{14}$$

which leads to Eq. (10), where only final plane wave states for the ejected nucleon are considered.

In the PWA and FSI calculations a single particle description is used. Bound state wave functions are taken from a Dirac-Hartree calculation [17] and are represented in Dirac four-spinor form. The current operators are treated in relativistic form and no nonrelativistic reduction is performed. The optical model Green's function is calculated as the solution of the Lippmann-Schwinger equation in momentum space to give the fully off-shell nucleon-nucleus T matrix.

The y scaling analysis presented in this paper will be performed for both (a) the relativistic plane wave approximation and (b) with the Green's function doorway approach to include the FSI. The two forms of the free electromagnetic current operator used are

$$\begin{aligned}\hat{J}^{\mu}_{cc2} &= F_1(q^2)\gamma^{\mu} + \imath\frac{F_2(q^2)}{2m}\sigma^{\mu\nu}q_{\nu},\\ \hat{J}^{\mu}_{cc1} &= G_m(q^2)\gamma^{\mu} - \frac{F_2(q^2)}{2m}\bar{\mathcal{K}}^{\mu}\\ &= F_1(q^2)\gamma^{\mu} + \imath\frac{F_2(q^2)}{2m}\sigma^{\mu\nu}\bar{q}_{\nu},\end{aligned} \tag{15}$$

where $G_m = F_1 + F_2$ is the familiar Sachs magnetic form factor and $\mathcal{K} \equiv k + k'$. The bars over $\bar{\mathcal{K}}$ and $\bar{q}$ indicate that k and k' are fixed to the on-shell values, e.g., $\bar{k}^0 \equiv \pm\sqrt{\mathbf{k}^2 + m^2}$, where the sign is dependent upon the $(\pm)$ character of the Dirac spinor. The definitions of $\hat{J}_{cc2}$ and $\hat{J}_{cc1}$ correspond to the $cc2$ and $cc1$ operators defined in Ref. [13]. Current conservation is imposed using the standard practice of replacing $\hat{q}\cdot\mathbf{J}$ by $q_0 J^0/|\mathbf{q}|$, but in general the current is not conserved by these two operators. These two forms of the nucleon current operator are equivalent in the on-shell limit and hence correspond to the same free nucleon electromagnetic currents. The difference is within the nuclear medium, where off-shell effects become important. The most general form of the current operator contains 12 independent terms, in which only two independent terms survive in the on-shell limit. To be able to construct the complete operator and the accompanying form factors would require a reliable off-shell nucleon structure model, for example a QCD based model. The differences between the $cc1$ and $cc2$ operators can only be fully understood microscopically with such a model. It can be stated that calculated differences associated with the differences between the $cc1$ and $cc2$ operators are derived from the underlying nucleon structure. For a thorough discussion and analysis of these two current operators and their underlying off-shell implications, please see Refs. [14–16].

Nonrelativistic calculations of FSI are constructed by removing all negative energy state contributions, which result from the Dirac dynamics in the relativistic calculation. This includes those negative energy contributions that arise from the construction of $\hat{U}_{\mathrm{opt}}$ and in the calculation of $\hat{G}_{\mathrm{opt}}$. This is the manner in which the nonrelativistic calculation is calculated here, where relativistic kinematics are maintained.

III. PWA AND FSI y SCALING RESULTS

In these and all subsequent calculations the full relativistic forms of the $cc1$ and $cc2$ current operators are used, where the free nucleon-nucleon form factors are taken from Ref. [18]. The bound state wave functions for the PWA and FSI calculations are from a Dirac-Hartree calculation [17]. In Eq. (15) one can see that the $cc1$ and $cc2$ forms of $\hat{J}^{\mu}$ are identical when $\mu = 0$, therefore in the calculation of R_L, the $cc1$ and $cc2$ versions give the same result. It can be shown that the longitudinal expressions derived for the $cc1$ and the $cc2$ cases in Ref. [13] are equivalent. For the transverse case the $cc1$ and $cc2$ expressions are not the same and will have different off-shell behavior, hence the transverse results

will be presented for both cases. In all of the figures, the curves labeled $cc1$ ($cc2$) use the $cc1$ ($cc2$) current operators in both the calculation of the transverse response function and in the calculation of the transverse nucleon structure function given in Eqs. (7) and (8) and used in the denominator of Eq. (4). In this paper all of the calculations are performed in momentum space and are for ^{40}Ca.

In Figs. 1–3 the PWA scaling functions are shown as a function of y for various values of the momentum transfer, $|\mathbf{q}|$. In Figs. 2 and 3 the transverse scaling functions are displayed using the $cc1$ and $cc2$ current operators, respectively. In the PWA calculations there is little dependence upon the different off-shell behavior of $cc1$ versus $cc2$, where the use of these two current operators gives very similar results. The transverse scaling function appears to scale reasonably well at the peak maximum and in the $y < 0$ tail region. The peak position shifts for $|\mathbf{q}| < 900$ MeV, but seems fixed at $y \approx 0$ for larger $|\mathbf{q}|$. In contrast in Fig. 1, $F_L(q,y)$ does not scale very cleanly. At the peak as $|\mathbf{q}|$ becomes larger, the peak height gradually increases and actually shifts slightly to lower y. The shift in the peak position may depend upon the particular choice of the y variable, but then a shift was not observed in the transverse calculation. The y scaling features are more clearly evident in Figs. 4–6, where slices of the scaling function at constant y are shown as a function of $1/|\mathbf{q}|$. As $|\mathbf{q}|^{-1}$ approaches zero, the scaling function should become constant. The upper panels show

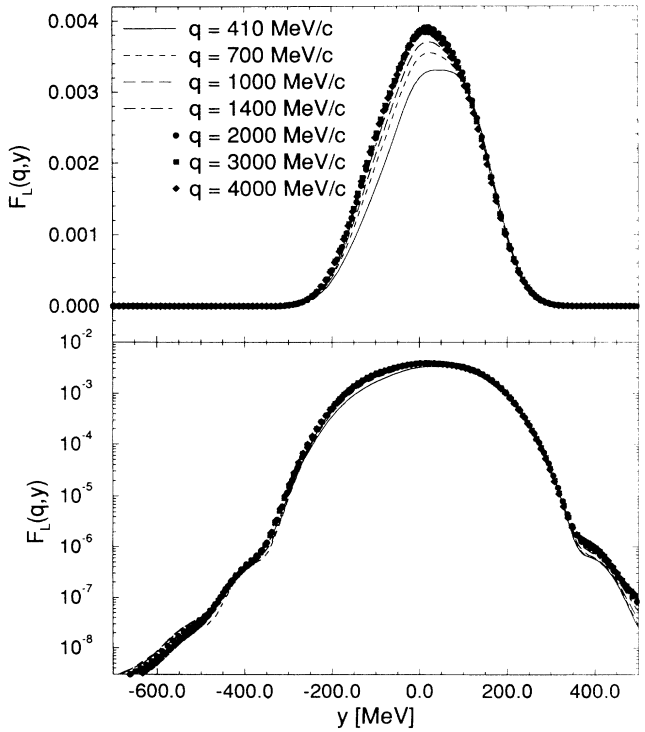

FIG. 1. The longitudinal scaling function $F_L(q,y)$ is calculated with the PWA calculation and shown with a linear scale (upper panel) and logarithmic scale (lower panel) for several values of the momentum transfer q as a function of the variable y.

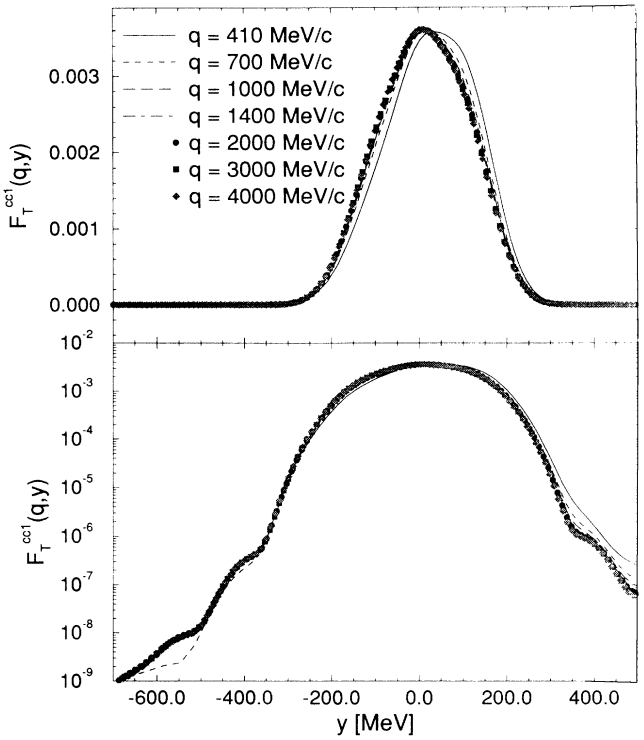

FIG. 2. The transverse scaling function $F_T^{cc1}(q,y)$ is calculated with the PWA calculation and shown with a linear scale (upper panel) and logarithmic scale (lower panel) for several values of the momentum transfer, q, as a function of the variable y. Here the $cc1$ current operator, as defined in Eq. (15), is used in both the calculation of the response functions and the nucleon structure function.

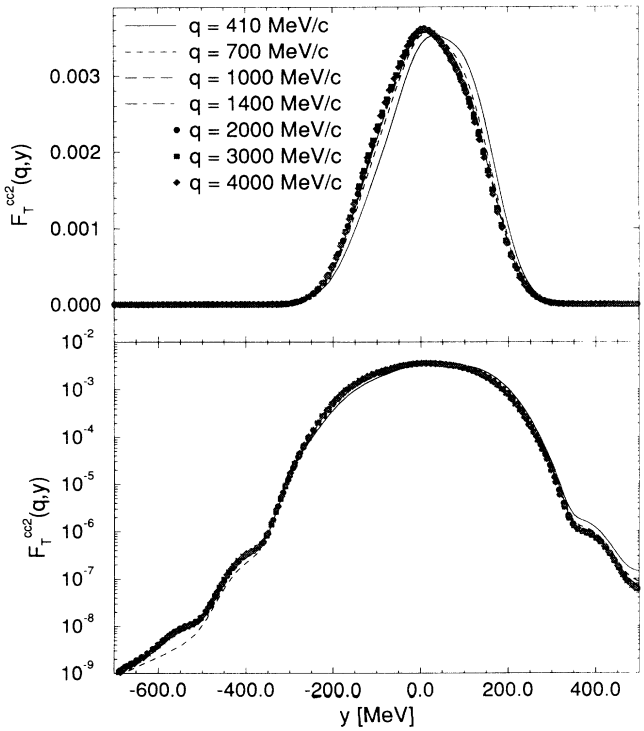

FIG. 3. The same as Fig. 2, except the $cc2$ current operator is used in these calculations.

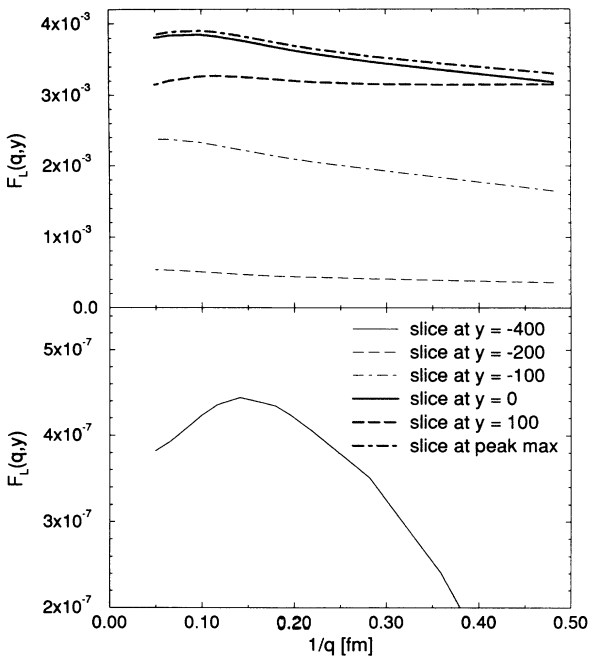

FIG. 4. Slices with constant y of the longitudinal scaling function are shown for the PWA calculation as a function of $|\mathbf{q}|^{-1}$ in fm. The upper panel shows slices for $y = -200, -100, 0, 100$ MeV and the peak maximum, while the lower panel shows the slice at $y = -400$ MeV on an expanded scale because this slice is much smaller.

the slices at $y = -200, -100, 0, 100$ MeV and at the peak maximum as a function of $|\mathbf{q}|^{-1}$, while the lower panel shows the slice at $y = -400$ MeV on a more expanded scale. For the transverse cases the scaling functions come relatively close to scaling. The slices at the peak maximum are nearly constant. The $y = 0$ slice scales almost as well as the peak maximum, where the deviation reflects the choice of the y variable. For improvements, corrections to y such as including effects due to the excitation energy of the residual nucleus may be required as well as other contributions [3]. The slice at $y = 100$ MeV does not scale as well, but the $y > 0$ region of $F_T(q, y)$ are affected greatly by the Δ resonance, which is not included in this calculation. The $y = -200$ MeV and $y = -400$ MeV slices appear to be approaching a scaling limit for $|\mathbf{q}|^{-1} \lesssim 0.1$ fm. In Fig. 4 the longitudinal scaling function does not appear to be approaching a scaling limit. As $|\mathbf{q}|^{-1}$ decreases, $F_L(q, y)$ increases until about $|\mathbf{q}|^{-1} \approx 0.1 - 0.15$ fm, where the scaling function changes behavior and begins to decrease. It seems clear that for the longitudinal case the PWA calculation does not approach a scaling limit.

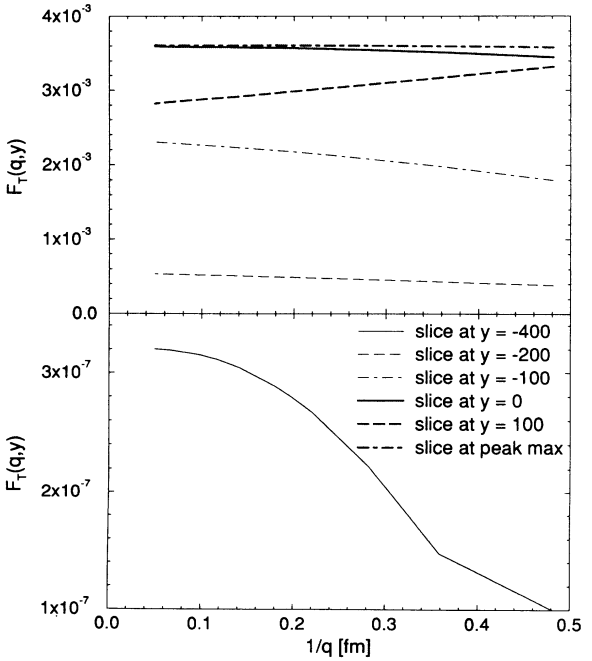

FIG. 5. The same as Fig. 4, except for the transverse scaling function calculated with the $cc1$ current operator.

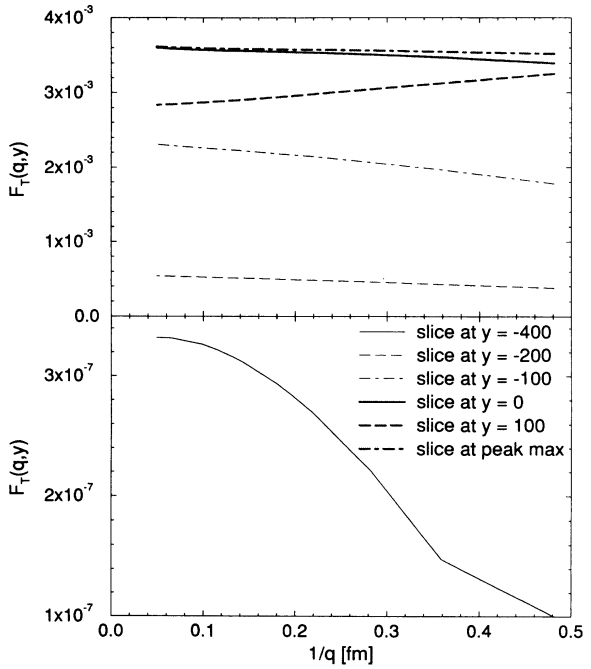

FIG. 6. The same as Fig. 4, except for the transverse scaling function calculated with the $cc2$ current operator.

Final state interactions are included using the Green's function doorway approach described above and in Ref. [8]. As in the PWA calculation, the $cc1$ and $cc2$ forms of the electromagnetic nucleon current operator are used and Dirac bound state wave functions are taken from Ref. [17]. Three different complex optical potentials are utilized to calculate the FSI. The global phenomenological Dirac optical potentials [BCL] of Ref. [19] and a Dirac impulse approximation [DIA] [20] are used. These two Dirac optical potentials incorporate contributions due to interactions with negative-energy states. Since negative-energy states are far off-shell, they may cause large differences to appear between the $cc1$ and $cc2$ operators [14]. A nonrelativistic impulse approximation [IA] is also used, which is basically a purely positive-energy version of the DIA [21]. The N-N potential, which is incorporated into the IA and DIA calculations, is taken

from Ref. [22] and extends up to 1000 MeV kinetic energies. The FSI results are calculated for momentum transfers between 410 and 1400 MeV/c. The optical potentials should be valid for nucleon kinetic energies up to 1000 MeV, which is larger than the ejectile kinetic energies at the quasielastic peaks considered. All of the calculations are performed in momentum space.

As was shown in Ref. [8], at large $|\mathbf{q}|$ the FSI continue to have a significant effect upon the calculations of the response functions. For momentum transfers between 410 and 1400 MeV/c the peak heights for the calculated longitudinal response function with FSI are about 0.7 times the peak heights in the corresponding PWA result, where this suppression is surprisingly consistent over the range of momentum transfers considered. There is also a slight shift in the position of the peak maximum to lower values of ω, as well as an overall change in the shape of the curve. It is clear that in the analysis of R_L and also R_T, the effects of the FSI continue to be significant at large $|\mathbf{q}|$.

The BCL, DIA, and IA optical potentials are used to calculate the FSI in Figs. 7, 8, and 9, respectively, where the scaling functions, F_L, F_T^{cc1}, and F_T^{cc2} are shown. In Fig. 9, the IA case is a nonrelativistic, positive-energy calculation, but uses the Dirac form of the $cc1$ and $cc2$ current operators.

The BCL optical potential is fitted phenomenologically to data up to initial proton kinetic energies of 1000 MeV, which is greater than the ejectile kinetic energies at the quasielastic peaks for all cases shown in Fig. 7. The FSI, represented by the BCL optical potential, have a large effect upon the scaling function, where there is a large suppression as compared to the PWA results. It is apparent that the scaling behavior is inferior to the results in the PWA calculations, especially for the transverse cases. The functions $F_L(y)$ and $F_T^{cc1}(y)$ do not scale very well, while $F_T^{cc2}(y)$, which uses the standard Dirac form for $\hat{J}^\mu$,

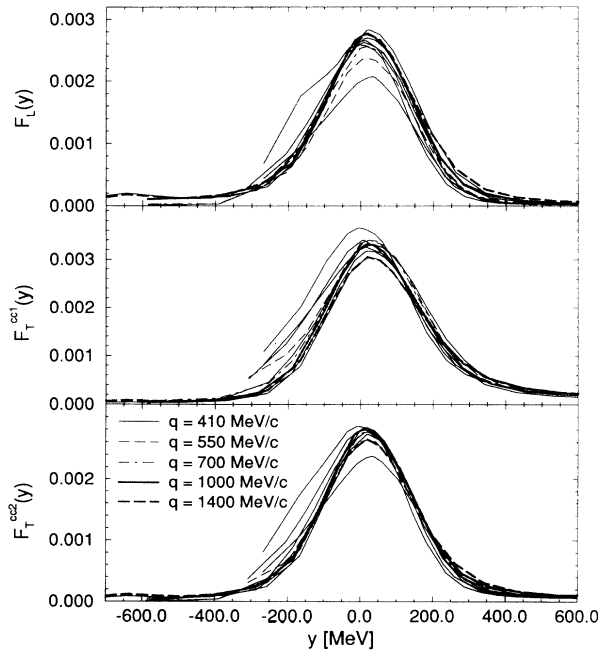

FIG. 7. The scaling functions, $F_L(q,y)$, $F_T^{cc1}(q,y)$, and $F_T^{cc2}(q,y)$ are shown in the upper, middle, and lower panels, respectively, resulting from calculations that include FSI using the relativistic BCL Dirac phenomenological optical potential [19]. The results are shown for several values of the momentum transfer, q, as a function of the y variable.

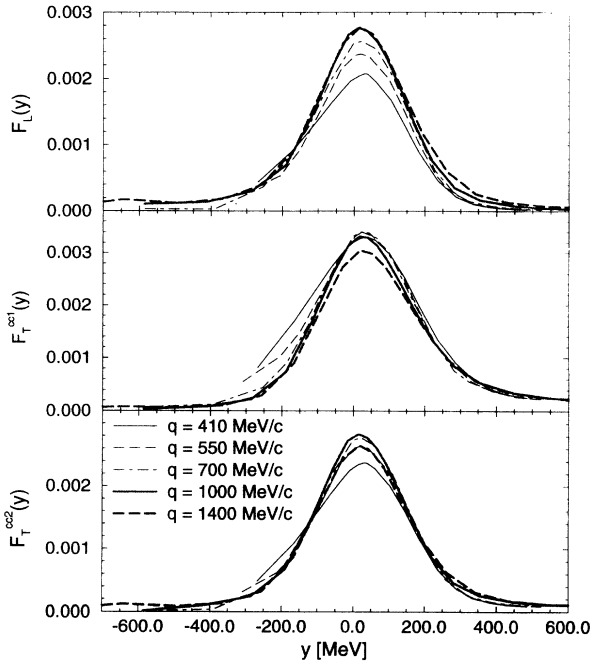

FIG. 8. The same as Fig. 7, except the Dirac impulse approximation [DIA] optical potential [20] is used to calculate the FSI contributions.

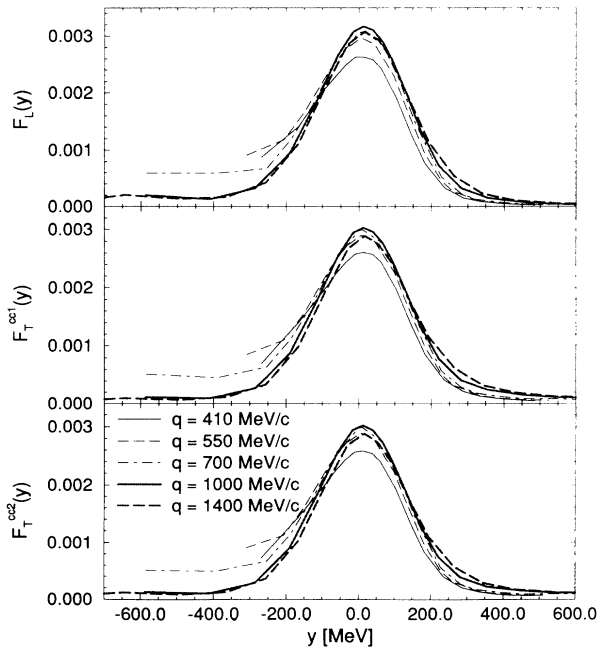

FIG. 9. The same as Fig. 7, except the nonrelativistic impulse approximation [IA] optical potential [21] is used to calculate the FSI contributions.

appears to approach a scaling limit for $|\mathbf{q}| > 700$ MeV/c.

The calculated separated response functions using the DIA optical potential for large values of ω (≥ 500 MeV) generally agree with the BCL results, but there exist some fluctuations. In elastic proton scattering, the observables are not sensitive to the interior of the nucleus and hence the interior scattering wave function plays only a passive role. In inclusive quasielastic (e,e') reactions inelastic channels contribute greatly, therefore the FSI model used here should be sensitive to the interior region of the ejectile wave function. This should also be reflected in differences between the $cc1$ and $cc2$ versions of $\hat{J}^\mu$, which give different off-shell contributions.

In Fig. 8 although there is a gross scaling behavior, this scaling behavior is worse than that seen in the PWA case and even the FSI results shown in Fig. 7. The longitudinal looks like it may scale for $|\mathbf{q}| \geq 1000$ MeV/c. The transverse results for both the $cc1$ and $cc2$ calculations appear to approach a scaling limit at $|\mathbf{q}| = 1000$ MeV/c, but then deviate sharply from scaling at $|\mathbf{q}| = 1400$ MeV/c. It may be that the FSI calculation is beginning to fail to be realistic at $|\mathbf{q}| = 1400$ MeV/c.

In the derivation of y scaling, relativistic dynamic degrees of freedom, specifically contributions from negative energy states, are not considered. The results shown in Fig. 9 do not include any negative-energy state contributions, and hence should be expected to give a reasonable scaling behavior. As $|\mathbf{q}|$ approaches 1000 MeV, the FSI results in Fig. 9 do appear to reach a reasonable scaling limit, much better than the results observed in Figs. 7 and 8. Again, the calculations at $|\mathbf{q}| = 1400$ MeV/c deviate from this scaling behavior, but nonrelativistic IA calculations are constructed from the same N-N interaction as the DIA calculations and therefore may also break down at $|\mathbf{q}| = 1400$ MeV/c. At this momentum transfer the quasielastic peak, and therefore the approximate ejectile kinetic energy, is about 800 MeV. One can see though that the inclusion of FSI, both relativistically and nonrelativistically, makes a y scaling analysis less clear.

IV. ANALYSIS OF FSI

When FSI are included in the analyses of y scaling it is clear that there are additional complications. There have been efforts to try and account for the effects of FSI, specifically by trying to understand the FSI contribution as a function of the three-momentum transfer, $|\mathbf{q}|$. By including a change of variables Eq. (12) can be expressed in momentum space as

$$\begin{aligned} T^{\mu\nu} &= \overline{\sum_i} \int \frac{1}{(2\pi)^3} d^3p d^3p' \langle i|\mathbf{p}-\mathbf{q}\rangle \hat{J}^\mu(q)^\dagger G(p,p') \\ &\quad \times \hat{J}^\nu(q)\langle \mathbf{p}'-\mathbf{q}|i\rangle \\ &= \overline{\sum_i} \int \frac{1}{(2\pi)^3} dE_p dY d\phi \frac{YE_p}{|\mathbf{q}|} dE_{p'} dY' d\phi' \frac{Y'E_{p'}}{|\mathbf{q}|} \\ &\quad \times \langle i|\mathbf{p}-\mathbf{q}\rangle \hat{J}^\mu(q)^\dagger G(p,p') \hat{J}^\nu(q)\langle \mathbf{p}'-\mathbf{q}|i\rangle, \quad (16) \end{aligned}$$

where the limits on $Y \equiv |\mathbf{p}-\mathbf{q}|$ and $Y' \equiv |\mathbf{p}'-\mathbf{q}|$ are

$$\sqrt{E_p^2 - m^2} - |\mathbf{q}| \leq Y \leq \sqrt{E_p^2 - m^2} + |\mathbf{q}|,$$
$$\sqrt{E_{p'}^2 - m^2} - |\mathbf{q}| \leq Y' \leq \sqrt{E_{p'}^2 - m^2} + |\mathbf{q}|.$$

The full many-body propagator is treated in the following fashion:

$$\begin{aligned} G(p,p') &\approx G_{\rm opt}(p,p') = G_0(p)\delta^3(\mathbf{p}-\mathbf{p}') \\ &\quad + G_0(p) T_{\rm opt}(p,p') G_0(p'). \quad (17) \end{aligned}$$

The δ function above can be expressed as

$$\delta^3(\mathbf{p}-\mathbf{p}') = \frac{|\mathbf{q}|}{YE_p} \delta(Y-Y')\delta(\phi-\phi')\delta(E_p - E_{p'}). \quad (18)$$

Combining Eqs. (16)–(18), the virtual Compton amplitude can be written in the following form:

$$T^{\mu\nu} = \frac{1}{|\mathbf{q}|} A(q) + \frac{1}{|\mathbf{q}|^2} B(q). \quad (19)$$

The first term corresponds to the PWA calculation, where if one ignores the q dependence in $A(q)$, the response functions should approximately scale as $|\mathbf{q}| \cdot R_{L,T}(y)$. The second term, which includes the FSI, varies as $|\mathbf{q}|^{-2}$ and should become smaller as $|\mathbf{q}|$ becomes large. In Refs. [2, 6] it was argued that by analyzing the scaling functions as a function of $|\mathbf{q}|^{-1}$, as $|\mathbf{q}|$ is increased the result should approach a scaling limit, where the FSI contributions become negligible.

In Fig. 10 the PWA and the three FSI calculations of the maximum of the peaks of the scaling functions are

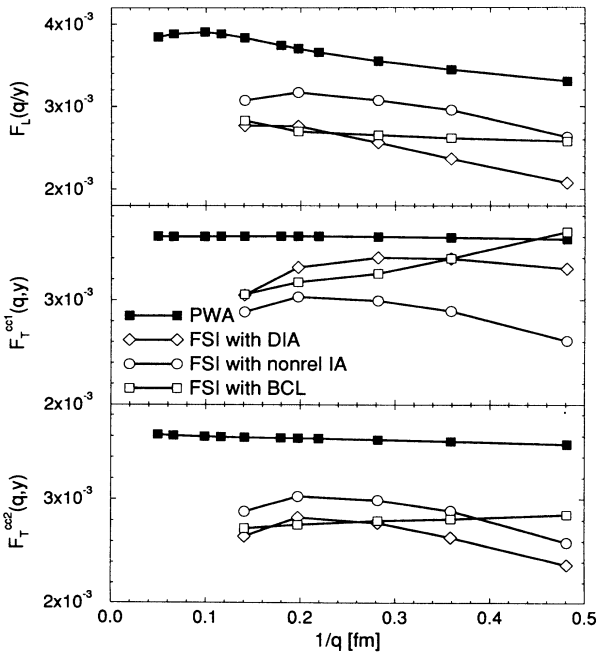

FIG. 10. The peak maxima for the scaling functions, $F_L(q,y)$, $F_T^{cc1}(q,y)$, and $F_T^{cc2}(q,y)$ are shown in the upper, middle, and lower panels, respectively. The results for the PWA and three FSI calculations are shown as a function of $|\mathbf{q}|^{-1}$ in fm.

shown for $F_L(q,y)$, $F_T^{cc1}(q,y)$, and $F_T^{cc2}(q,y)$ as a function of $|\mathbf{q}|^{-1}$. As mentioned earlier, one can clearly see here how the PWA transverse results approach a constant limit at small values of $|\mathbf{q}|^{-1}$, while the longitudinal results increase as $|\mathbf{q}|^{-1}$ reaches 0.1 fm and then decrease as $|\mathbf{q}|^{-1}$ is reduced further.

As argued in Refs. [2, 6], the FSI contributions should behave approximately as $|\mathbf{q}|^{-2}$ and therefore the FSI effects in the scaling function should vanish for very large values of $|\mathbf{q}|$. It should be first noted that even at the largest values of $|\mathbf{q}|$ considered here, the FSI contributions cause a large suppression of the separated scaling functions and hence the response functions for both the longitudinal and transverse cases, therefore a reduction in the effects of FSI is not observed at any momentum transfer.

In analyzing the scaling behavior, the nonrelativistic IA calculation of the FSI contributions, represented by the open circles in Fig. 10, appear to be reaching a scaling limit at $|\mathbf{q}| \approx 1000$ MeV. The points calculated at $|\mathbf{q}| = 1400$ MeV violate this scaling tendency, but at this large momentum this violation may be due to limits in the accuracy of this particular FSI calculation. This scaling behavior is observed for $F_L(q,y)$ as well as the two transverse cases.

The relativistic DIA calculation, given by the open diamonds in Fig. 10, does not appear to scale as well as the PWA or the nonrelativistic IA curves. The $cc2$ transverse result looks like it may scale, except for the 1400 MeV point, but the $cc1$ result does not scale here. The open squares correspond to the use of the BCL Dirac optical potential, which should give the most physical representation of the FSI. It appears that this calculation does not scale at the peak for any of the three scaling functions. It may be that one must extend the calculation to larger values of $|\mathbf{q}|$ before the scaling limit is obtained, but since y scaling is a nonrelativistic construct, one should not really expect a theory which incorporates relativistic dynamical effects to rigidly obey y scaling.

Equation (19) suggests that the scaling functions should behave linearly for very small values of $|\mathbf{q}|^{-1}$. The PWA results in Figs. 5, 6, and 10 are linear. The IA and DIA FSI results do not appear linear, but may become linear at larger $|\mathbf{q}|$. Interestingly, the BCL FSI results are very close to being linear for all three scaling functions and over the whole range of momentum transfer considered. One should expect though that the FSI results should be linear and approach the PWA result for $|\mathbf{q}|^{-1} = 0$. This is clearly not the case for the results shown in Fig. 10 for the peak maxima. For values of $y < 0$ the linear behavior is not clear. For $y = -100$ MeV there is no evidence of any linear approach to the PWA result; at $y = -200$ MeV the FSI results appear to be converging to the PWA value at $|\mathbf{q}|^{-1} = 0$, but this may be a result of the tails of the scaling functions all becoming very small.

A similar sort of violation can be seen in the concept of the Coulomb sum rule [23–25], which is also a nonrelativistic construction. When one includes relativistic dynamics into the PWA calculation, instead of the Coulomb sum rule limit of one or Z, one finds the relativistic limit of $\frac{1}{2}$ or $Z/2$.

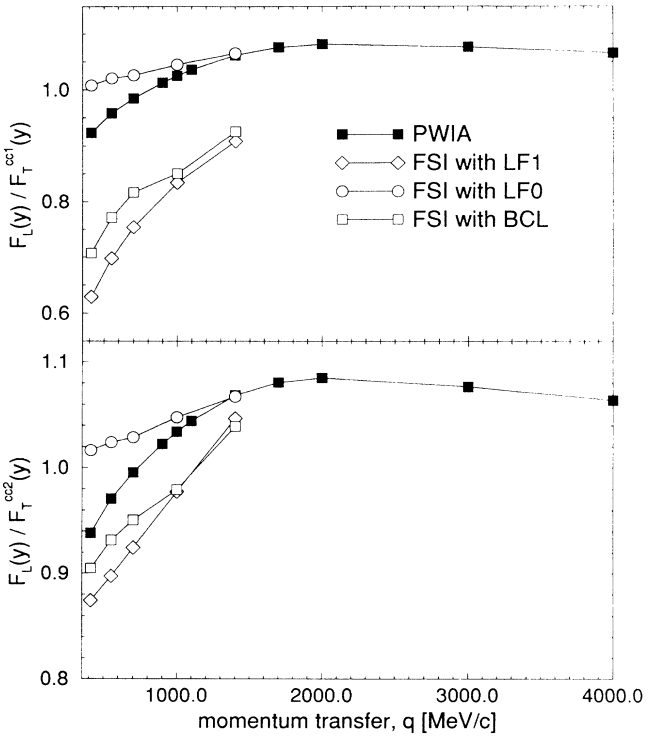

FIG. 11. The ratios, $F_L(q,y)/F_T^{cc1}(q,y)$ and $F_L(q,y)/F_T^{cc2}(q,y)$, of the peak maxima are shown in the upper and lower panels, respectively, as a function of the momentum transfer, $q = |\mathbf{q}|$ in MeV/c. Results are given for the PWA and the three FSI calculations.

From y scaling it is expected that the longitudinal and transverse scaling functions should be approximately equal, which is derived from the idea that the scaling functions are related to the nucleon momentum distribution inside the nucleus. The ratios, $F_L(y)/F_T(y)$, for the peak maxima are shown in Fig. 11 for both the $cc1$ and $cc2$ calculations. For $|\mathbf{q}|$ larger than 1000 MeV, the PWA and IA calculations give ratios that are greater than 1.05. The relativistic FSI calculations are less than 1 for the $cc1$ case and become greater than 1 as $|\mathbf{q}|$ increases when the $cc2$ current operator is used. Although y scaling is derived in a nonrelativistic plane wave limit to give the nucleon momentum distribution, the PWA results given in Fig. 11 indicate that some of the y scaling assumptions and approximations may not be completely valid.

V. SUMMARY AND CONCLUSION

The separated scaling functions derived from y scaling are calculated in both a plane wave approximation calculation and with a model which uses the optical model Green's function approach to include final state interactions. Two relativistic Dirac optical potentials and a nonrelativistic optical potential are used to construct the final state interactions. The nonrelativistic IA calculation of FSI does seem to give a reasonable degree of scal-

ing, when compared to the PWA calculation, although the effect of the FSI remains strong. When relativistic Dirac dynamical degrees of freedom, specifically contributions from negative energy states, are included into the calculation of FSI, there is no confident level of y scaling evident.

For large momentum transfers it has been suggested that the role of FSI may be reduced, and that by investigating the scaling functions as a function of $|\mathbf{q}|^{-1}$ it may be possible to remove the effects of FSI altogether [2]. It is found in the model calculation performed in this paper that this is not true, that the effects of FSI remain strong at all of the momentum transfers considered, in agreement with the conclusions of Ref. [6]. This is especially true for the relativistic case, where the model calculations which include relativistic FSI do not exhibit scaling.

ACKNOWLEDGMENTS

The author would like to acknowledge the graciou hospitality of the Service de Physique et Techniques Nucléaires at the Centre d'Etudes de Bruyères-le-Châtel, where much of this work was performed. The author would also like to thank R. M. Thaler for a critical reading of the manuscript. This work was performed in part under the auspices of the U. S. Department of Energy under contracts No. DE-AC05-84OR21400 with Martin Marietta Energy Systems, Inc., and DE-FG05-87ER40376 with Vanderbilt University. This research has been supported in part by the U.S. Department of Energy, Office of Scientific Computing under the High Performance Computing and Communications Program (HPCC) as a Grand Challenge titled the Quantum Structure of Matter.

[1] For excellent reviews please see Refs. [3] and [2].
[2] C. Ciofi degli Atti, E. Pace, and G. Salmè, Phys. Rev. C **43**, 1155 (1991).
[3] D. B. Day, J. S. McCarthy, T. W. Donnelly, and I. Sick, Ann. Rev. Nucl. Part. Sci. **40**, 357 (1990).
[4] I. Sick, Comments Nucl. Part. Phys. **18**, 109 (1988).
[5] T. Uchiyama, A. E. L. Dieperink, and O. Scholten, Phys. Lett. B **223**, 31 (1989).
[6] S. A. Gurvitz and A. S. Rinat, Phys. Lett. B **197**, 6 (1987); A. S. Rinat and R. Rosenfelder, *ibid.* **193**, 411 (1987).
[7] Y. Horikawa, F. Lenz, and N. C. Mukhopadhyay, Phys. Rev. C **22**, 1680 (1980).
[8] C. R. Chinn, A. Picklesimer, and J. W. Van Orden, Phys. Rev. C **40**, 790 (1989).
[9] S. A. Gurvitz and A. S. Rinat, Phys. Rev. C **35**, 696 (1987).
[10] I. Sick, D. Day, and J. S. McCarthy, Phys. Rev. Lett. **45**, 871 (1980).
[11] Z.-E. Meziani *et al.*, Phys. Rev. Lett. **69**, 41 (1992).
[12] R. Cenni, C. Ciofi degli Atti, and G. Salmè, Phys. Rev. C **39**, 1425 (1989).
[13] T. de Forest, Nucl. Phys. **A392**, 232 (1983).
[14] C. R. Chinn and A. Picklesimer, Il Nuovo Cimento **105A**, 1149 (1992).
[15] H. W. L. Naus and J. H. Koch, Phys. Rev. C **36**, 2459 (1987).
[16] P. C. Tiemeijer and J. A. Tjon, Phys. Rev. C **42**, 599 (1990).
[17] C. J. Horowitz and B. D. Serot, Nucl. Phys. **A368**, 503 (1981).
[18] M. Gari and W. Krumpelmann, Phys. Lett. **173B**, 10 (1986).
[19] R. H. McCamis *et al.*, Phys. Rev. C **33**, 1624 (1986); E. D. Cooper, B. C. Clark, S. Hama, and R. L. Mercer, Phys. Lett. B **206**, 588 (1988); *ibid.* **220**, 658(E) (1989).
[20] M. V. Hynes, A. Picklesimer, P. C. Tandy, and R. M. Thaler, Phys. Rev. C **31**, 1438 (1985).
[21] A. Picklesimer, P. C. Tandy, R. M. Thaler, and D. H. Wolfe, Phys. Rev. C **30**, 1861 (1984).
[22] M. A. Franey and W. G. Love, Phys. Rev. C **31**, 488 (1985).
[23] C. R. Chinn, A. Picklesimer, and J. W. Van Orden, Phys. Rev. C **40**, 1159 (1989).
[24] T. C. Ferée and D. S. Koltun, Phys. Rev. C **49**, 1961 (1994).
[25] G. Do Dang, M. L'Huillier, Nguyen Van Giai, and J. W. Van Orden, Phys. Rev. C **35**, 1637 (1987).